Earth and Planetary Science Letters 290 (2010) 214–223

Contents lists available at ScienceDirect

Earth and Planetary Science Letters

journal homepage: www.elsevier.com/locate/epsl

The seismic-stratigraphic record of lake-level fluctuations in Lake Challa: Hydrological stability and change in equatorial East Africa over the last 140 kyr

J. Moernaut [a,*], D. Verschuren [b], F. Charlet [a], I. Kristen [c], M. Fagot [b], M. De Batist [a]

[a] Renard Centre for Marine Geology, Ghent University, Ghent, Belgium
[b] Limnology research group, Ghent University, Ghent, Belgium
[c] Climate Dynamics and Sediments, GeoForschungsZentrum Potsdam, Potsdam, Germany

ARTICLE INFO

Article history:
Received 28 September 2009
Received in revised form 30 November 2009
Accepted 8 December 2009
Available online 13 January 2010

Editor: P. DeMenocal

Keywords:
equatorial East Africa
Indian Ocean monsoon
lake level
seismic stratigraphy

ABSTRACT

Seismic-reflection data from crater lake Challa (Mt. Kilimanjaro, equatorial East Africa) reveal a ~210-m thick sedimentary infill containing distinct seismic-stratigraphic signatures of late-Quaternary lake-level fluctuations. Extrapolation of a well-constrained age model on the cored upper part of the sequence suggests that these lake-level fluctuations represent a detailed and continuous record of moisture-balance variation in equatorial East Africa over the last 140 kyr. This record indicates that the most severe aridity occurred during peak Penultimate glaciation immediately before ~128 kyr BP (coeval with Heinrich event 11) and during a Last Interglacial 'megadrought' period between ~114 and ~97 kyr BP; in comparison, Last Glacial Maximum (LGM) aridity was modest. It was preceded by ~75 000 years of relatively stable and moist climate conditions interrupted by eleven short-lived dry spells, five of which match the timing of Heinrich events 2 to 6. Climate history near the East African equator reflects variation in the precessional forcing of monsoon rainfall modulated by orbital eccentricity, but precession-driven moisture fluctuations were less extreme than those observed in northern and southern tropical Africa. The near-continuous moist climate from ~97 to 20.5 kyr BP recorded in the Lake Challa record contrasts with the trend towards greater aridity after ~70 kyr BP documented in equatorial West Africa. This long period of moist glacial climate and a short, relatively modest LGM drought can be attributed to greater independence of western Indian Ocean monsoon dynamics from northern high-latitude glaciation than those in the tropical Atlantic Ocean. This rather persistent moist glacial climate regime may have helped maintain high biodiversity in the tropical forest ecosystems of the Eastern Arc mountains in Tanzania.

1. Introduction

High-resolution, continuous climate records from (sub-)tropical continental regions are beginning to produce a detailed picture of low-latitude climate variability through the last glacial–interglacial cycle, and reveal a spatially variable combination of local and long-distance climate forcing. Records of the East Asian Monsoon in subtropical China (Yuan et al., 2004; Kelly et al., 2006; Wang et al., 2008) and of the tropical Atlantic monsoon in northwest Africa (Tjallingii et al., 2008) both highlight the decreasing amplitude of orbital-scale monsoon variations over the course of the last glacial period, and the significance of millennial-scale episodes of weak monsoon activity. The long-term trend reflects the decreasing amplitude of precessional insolation forcing from ~125 to ~25 kyr BP, with a distinctly muted signature in the period 60–25 kyr BP (~Marine Isotope Stage 3, MIS3) when orbital eccentricity reached a minimum (Berger and Loutre, 1991). The most pronounced East Asian and West African weak monsoon episodes during MIS3 tend to match the timing of Heinrich events (Wang et al., 2001; Tjallingii et al., 2008), pointing to the long-distance impact of episodic North Atlantic cooling and iceberg discharge on Atlantic meridional overturning circulation (cf. McManus et al., 2004) and on northern Eurasian temperature (Ganopolski and Rahmstorf, 2001). This long-distance impact is also evident throughout much of the African continent (Brown et al., 2007; Lamb et al., 2007; Tierney et al., 2008; Thomas et al., 2009), but whether it resulted mostly from greater southward displacement of the Intertropical Convergence Zone (ITCZ) during stadials (Brown et al., 2007) or Indian Ocean cooling (Tierney et al., 2008) is as yet uncertain.

African lake records spanning the complete last glacial–interglacial cycle (Scholz et al., 2007; Cohen et al., 2007) have now also revealed evidence for major orbital-scale climate fluctuation during MIS 5 (130–74 kyr BP), when orbital eccentricity, and thus the amplitude of precessional forcing, was high. In southeastern tropical Africa, where the Lake Malawi record (10° S) has excellent continuity and resolution, prolonged aridity dated to the late Penultimate Glaciation

* Corresponding author.
E-mail address: Jasper.Moernaut@ugent.be (J. Moernaut).

0012-821X/$ – see front matter © 2009 Elsevier B.V. All rights reserved.
doi:10.1016/j.epsl.2009.12.023

(~135–127 kyr BP) and to part of MIS5 (~115–95 kyr BP) was significantly more severe than the 'benchmark' dry climate of the Last Glacial Maximum (LGM). The Lake Malawi region also experienced two lesser droughts at ~78–74 kyr BP and ~64–62 kyr BP, before recovering to a relatively stable moist climate regime persisting until the LGM. This characteristic moisture-balance evolution could thus far not be properly assessed beyond southeastern tropical Africa, because of hiatuses in other available lake records, including lakes Tanganyika in central Africa (6°S; Scholz et al., 2007; McGlue et al., 2008), Bosumtwi in tropical West Africa (6°N; Scholz et al., 2003, 2007) and Lake Naivasha (0°45'S) in equatorial East Africa (Trauth et al., 2003).

In this study, we use seismic-reflection signatures of past lake-level fluctuation in Lake Challa (Kenya/Tanzania) to reconstruct a continuous moisture-balance record from near the equator in East Africa over the past 140 kyr. This site's location provides unique information on how rainfall contributions from both southeasterly and northeasterly monsoons in the western Indian Ocean, coupled with a fairly modest amplitude of long-term variation in local insolation compared to that at northern and southern subtropical latitudes (Berger and Loutre, 1991) and a relative modest influence from northern high-latitude ice-sheet dynamics (Verschuren et al., 2009) have shaped the region's climate history.

2. Setting and data acquisition

Lake Challa (3.3° S; 37.7° E) is a 4.2 km² volcanic crater lake at 880 m altitude on the lower East slope of Mt. Kilimanjaro. It was 94 m deep at the time of our seismic survey, but during the period 1999–2008 has varied between 92 and 98 m. Twice-yearly passage of peak insolation, and hence the zone of maximum convective activity, over the region creates a bimodal pattern of seasonal rainfall, with the southeasterly monsoon bringing 'long rains' from March to mid-May and the northeasterly monsoon bringing 'short rains' from late October to December (Fig. 1). The local climate is tropical semi-arid, with monthly mean daytime temperatures ranging from 26 °C in July–August to 30 °C in February–March, a total annual rainfall of ~565 mm, and ~1735 mm lake-surface evaporation. The lake's water budget is also influenced by sub-surface in- and outflow. Sub-surface inflow originates from rainfall on the upper flanks of Mt. Kilimanjaro. Surface inflows are limited to run-off from the steep inner crater slopes except for a narrow, ~300-m long ravine which breaches the crater's northwestern rim and is active during infrequent heavy thunderstorms. Sub-surface outflow is estimated to amount to ~2.5% of lake volume annually (Payne, 1970). More significant outflow through porous upper crater walls probably starts ~10 m above the 2003 lake level, the upper limit of shallow caves eroded by wave action during past highstands. A dry, boulder-strewn tributary creek situated immediately above the springs which feed the Kirimeri stream ~1 km east of Challa crater testifies to an episode when spring discharge was much higher than today, likely reflecting higher lake outflow rates during a historical highstand.

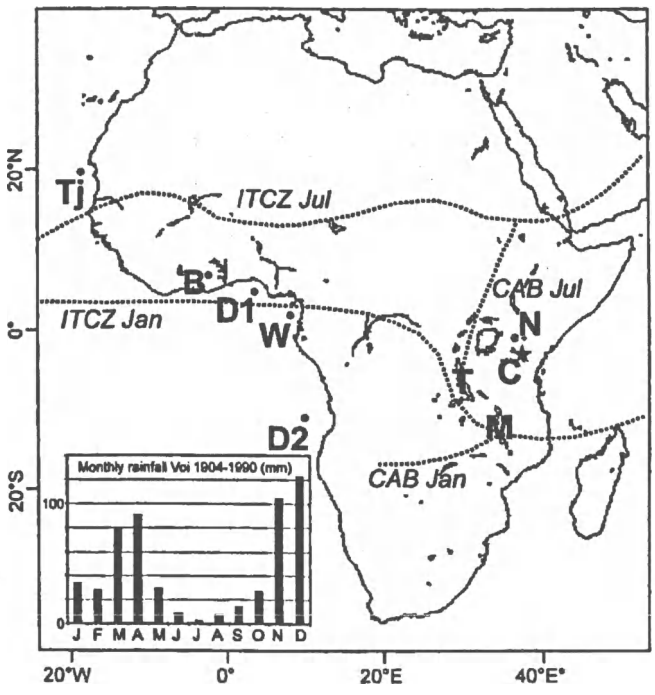

Fig. 1. Outline map of Africa with indication of the January and July positions of the Intertropical Convergence Zone (ITCZ), the Congo Air Boundary (CAB) where the Atlantic and Indian Ocean moisture converges, and the location of key sites discussed in this paper: lakes Challa (C), Bosumtwi (B), Tanganyika (T), Naivasha (N) and Malawi (M), and the marine records of Tjallingii et al. (2008) (Tj), Weldeab et al. (2007) (W) and Dupont et al. (2000) (D1: GIK 16856 and D2: Geo8 1016). The inset shows the seasonal distribution of monthly rainfall at Voi, ~90 km east of Challa.

In 2003 we acquired a dense (37 km) grid of high-resolution reflection-seismic profiles (Fig. 2A) using a 3.5 kHz Geopulse pinger system mounted on a double-hulled inflatable platform with an electric outboard engine. The acoustic signal penetrated a 270 ms two-way travel time (TWT) of lacustrine sediments, corresponding to a total thickness of ~210 m, with a vertical resolution of 10–20 cm. Navigation and positioning were achieved by GPS. All data were digitally recorded on a Triton-Elics Delph-2 acquisition system (sampling frequency: 20 kHz; shooting rate: 0.6 s), with application of a bandpass filter of between 600 and 3600 Hz. Seismic interpretation was done using the SMT Kingdom Suite 7.5 package. In 2005 we recovered three parallel UWITEC piston cores of 20–22 m length and two surface gravity cores at a mid-lake location (Fig. 2). These together form a 21.65-m long composite profile of fine-grained lake muds composed mainly of diatom silica, organic matter, carbonate and eolian mineral inputs. The sequence is interrupted by five turbidites (26, 34, 5, 6 and 15 cm thick) consisting largely of re-deposited crater slope material. This cored upper part of the Lake Challa record represents the last 25 000 years of lake history. Our age-depth model for this cored sequence is a smoothed spline through the INTCAL04-calibrated AMS ^{14}C dates of 164 bulk organic carbon samples, corrected for a lake-carbon reservoir age which varies with depth between ~200 and ~450 years (Verschuren et al., 2009).

3. Seismic-stratigraphic analysis and dating

The bathymetric map (Fig. 2A) shows the typical morphology of a volcanic crater basin with upper slopes dipping between ~30° and the near-vertical, separated from the gently dipping (1–5°) basin-plain periphery and flat central lake floor by a sharp slope break at ~60–70 m depth. The densely spaced 2D seismic profiles permitted a pseudo-3D reconstruction of the sedimentary infill (Fig. 2B), which reveals that the crater basin was originally divided in three areas of deposition (D1–D3) separated by two central rock cones (Fig. 2B and Supplementary Fig. S1), likely consisting of rapidly accumulated volcanic tuff. These cones have substantially influenced the present-day topography of the lower ~2/3 of the sedimentary infill, due to site-specific differences in total compaction between the thick sediment package in the three depressions and the thinner sediment package above the central tuff cones. This is clearly indicated in seismic-stratigraphic U11 (Fig. 3), where the location of reflector onlap above D2 is at a lower absolute elevation than the continuous reflectors in the lake centre. This site-specific compaction hampers the reconstruction of the lake paleo-bathymetry for the early part of lake history.

Analysis of reflection terminations and acoustic facies aided by facies thickness measurements and isopach maps allow discrimination of 13 finely-stratified seismic-stratigraphic units (Fig. 3), each

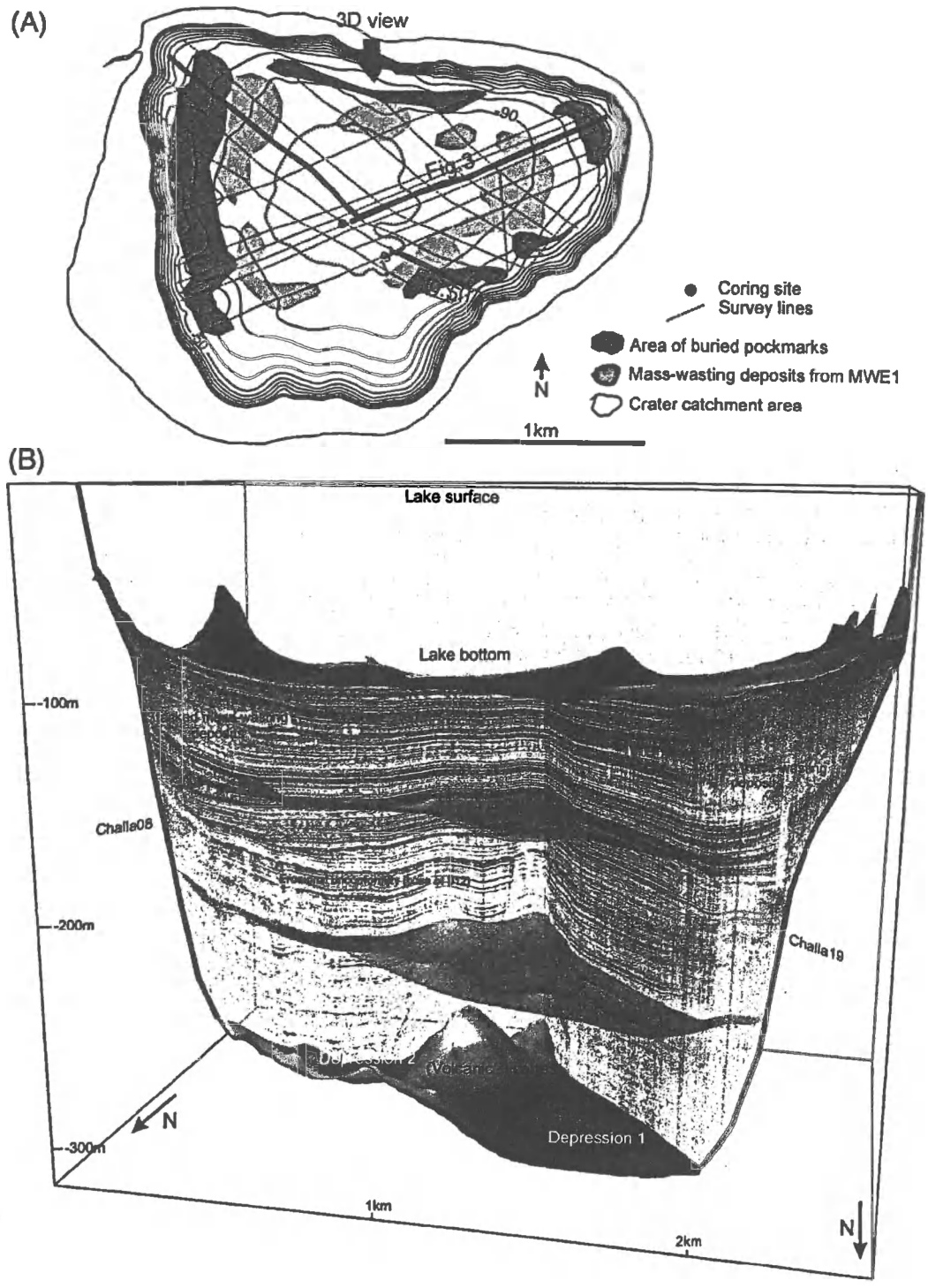

Fig. 2. A) Lake Challa and its crater catchment area, with bathymetry, location of the principal core site in relation to seismic survey lines, and the spatial distribution of mass-wasting event 1 (MWE1) deposits and buried pockmarks at this stratigraphic level. Bathymetry was constructed using the seismic profiles and echosounder data. Depth contour lines are drawn at 10-m intervals to 90 m depth, followed by a 4-m interval to 94 m. B) 3D representation of Lake Challa's sedimentary infill, of which the upper half (above 'erosional unconformity') is studied in this paper, viewed from the north and cut at seismic lines 8 and 19 (red lines in A). The lower- and uppermost surface represent the crater basement and lake bottom, respectively. The other, virtual surfaces were created by the interpolation between arbitrary seismic reflectors to illustrate the gradual leveling of basement topography by the sedimentary infill, although site-specific differences in total compaction also influenced the present-day topography of those surfaces. Colors indicate their relative depth, ranging from purple (deepest) to red (shallowest). (For interpretation of the references to color in this figure legend, the reader is referred to the web version of this article.)

displaying one of two dominant patterns of sediment deposition. Units 1, 2, 4, 5, 7, 12 and 13 are characterized by uniform draping with little lateral thickness variation between the basin plain and the basin-plain periphery. Units 3, 6, 8, 9, 10 and 11 are characterized by basin-focused (ponded) sedimentation; focusing is strong in Units 11 and 9, and moderate in Units 3, 6, 8 and 10. In the basin plain these ponded units are concordant with adjacent draped units, but onlapping reflector terminations at the basin-plain periphery characterize their confined depositional areas, clearly illustrated by isopach maps (Fig. 4; Supplementary Fig. S1). These isopach maps are not affected by site-specific differences in total compaction caused by basement topography, and therefore provide more reliable information on

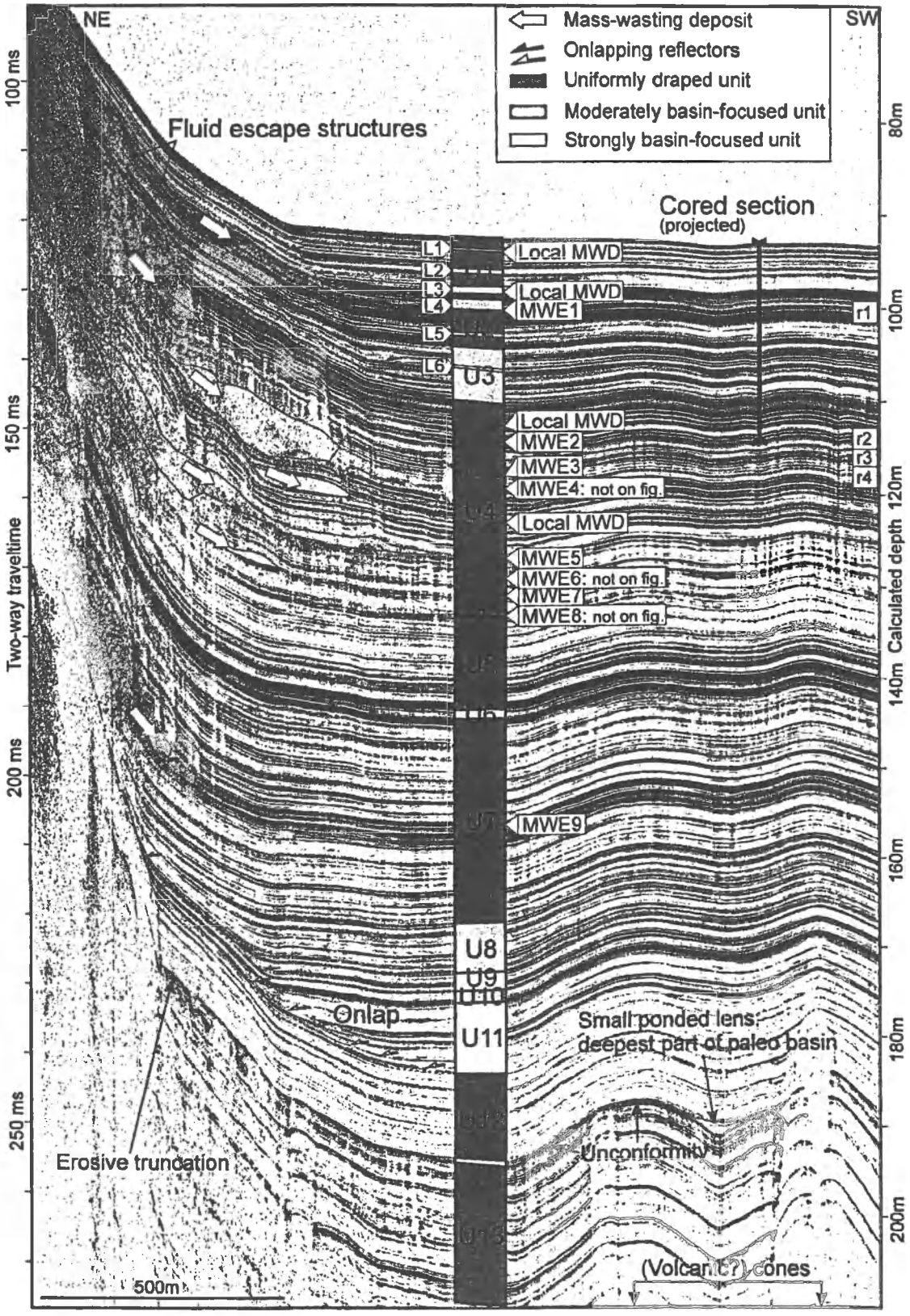

Fig. 3. Upper half of Lake Challa's sedimentary infill with indication of seismic units and their geometry, the stratigraphic position of mass-wasting events (MWE) and local mass-wasting deposits (MWD), and projection of the sediment core onto the seismic profile. r1 to r4 represent the seismic reflectors corresponding to the stratigraphic levels of MWE1 to MWE4. Small ponded lenses (L) occur within U1–U3. L1–5 occur within Units 1 and 2, both characterized by predominantly draped sedimentation; L6′ occurs within Unit 3, characterized by moderately basin-focused sedimentation (see also Supplementary Fig. S2). Used acoustic velocity is 1500 m/s for U1–U6, 1550 m/s for U7–U12.

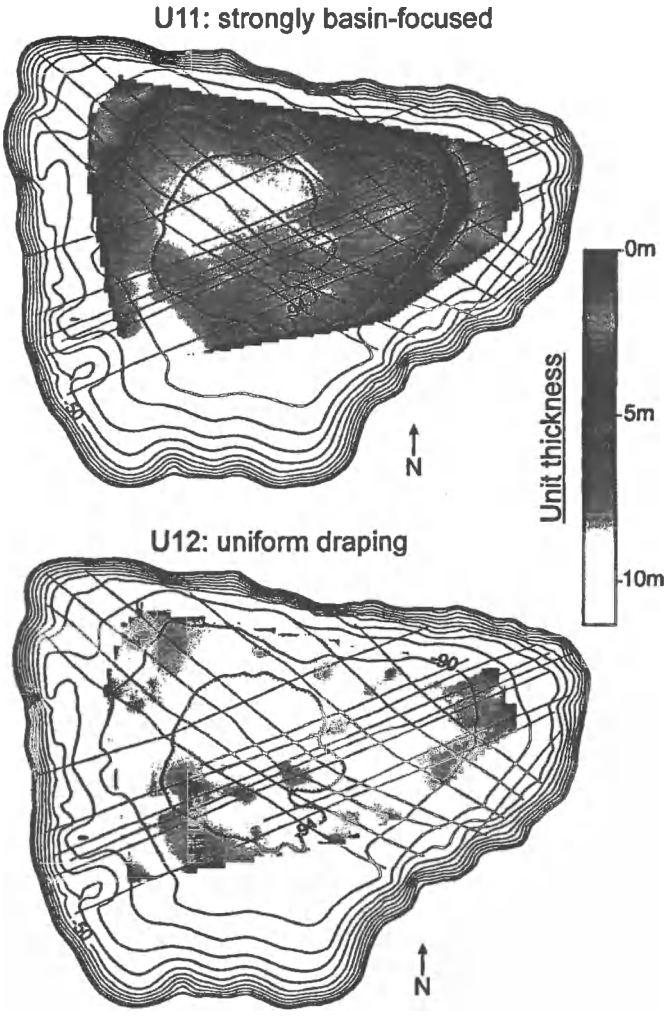

Fig. 4. Isopach maps showing the difference in depositional geometry between the uniformly draped Unit 12 and the strongly focused Unit 11. The small red patches in Unit 12 are due to the locally pronounced morphology of the erosional unconformity below it. Isopach maps for the other seismic units are presented in Supplementary Fig. S1.

depositional geometries and processes than iso-depth maps of single stratigraphic horizons. The uppermost units (U1–U3) also reveal several small (0.15 m–1.3 m thick) ponded lenses (L1–L6′) with a mostly low-amplitude acoustic facies (Supplementary Fig. S2).

Near the basin-floor periphery, numerous mass-wasting deposits (MWDs) can be identified on the basis of their transparent-to-chaotic facies smoothly intercalated between continuous reflectors, their associated landslide scarps and frontal ramps (Fig. 3; Moernaut and De Batist, submitted for publication). These features indicate that the MWDs result from failure of sublacustrine sedimentary slopes. At nine stratigraphic levels, several such mass-wasting deposits occur (Fig. 3), indicating that multiple slope failures took place at a basin-wide scale in a very short period; we identify these as mass-wasting events (MWE). At four other stratigraphic levels, evidence for mass wasting is limited to observations of a single MWD.

Buried fluid-escape structures, such as pockmarks and fluid conduits, are omnipresent at the basin-floor periphery. The fluid conduits are rooted in buried MWDs, which are emplaced on top of undisturbed sediment sequences (Fig. 5), indicating that they are probably not created by hydrothermal circulation from the crater basement. Also, most pockmarks are buried by U1 (Fig. 5), implying that almost no fluid expulsion has occurred since the start of U1 deposition. MWE1 seems to be temporally and spatially linked to this

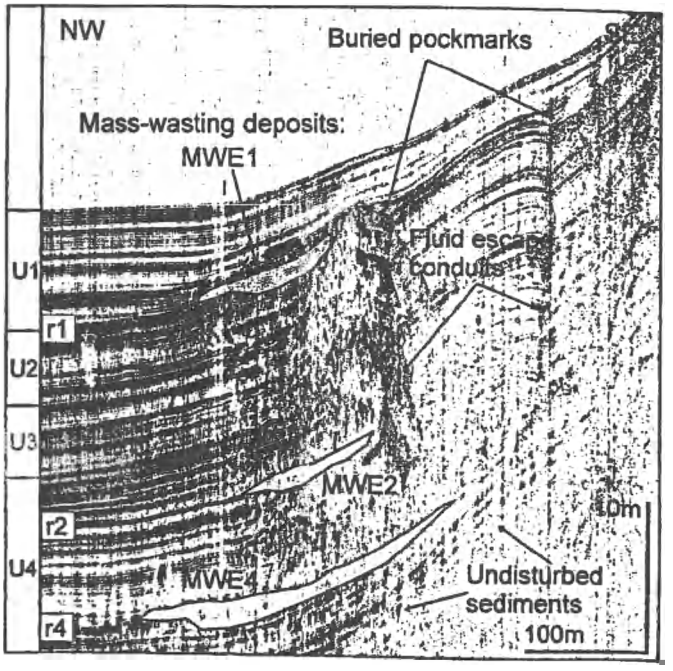

Fig. 5. Uppermost seismic stratigraphy showing buried fluid-escape structures and mass-wasting deposits (transparent white). r1 to r4 correspond to the same stratigraphic levels as in Fig. 3. Two large fluid conduits are rooted at the top of MWE4 or at the lateral continuation of its stratigraphical position, and are buried by U1 sediments.

period of focused fluid escape or to its abrupt cessation, suggesting that they could also be genetically linked.

An irregular high-amplitude reflector at ~100 m sub-bottom depth, marking the U13–U12 boundary, forms an erosional unconformity that locally truncates underlying reflectors. It is associated with massive sediment disturbances/displacements, fluid-escape structures, and a localized cover of thin ponded lenses (Fig. 3; Supplementary Figs. S3 and S4). Taking into account site-specific total compaction above basement topography, these lenses were likely deposited in the deepest parts of that period's paleo-basins.

The four uppermost seismic units correlate tightly to variations in core lithology and water content (Fig. 6A). MWE1, MWE2 and two local MWDs are each tied to a turbidite, and the ponded unit U3 is tied to a core section with lower water content. Cored seismic units with different spatial geometry also differ in mean linear accumulation rate, with as end-members the ponded Unit 3 (1.0 mm/yr) and the draped Unit 2 (0.68 mm/yr); the draped Unit 4 has an intermediate mean accumulation rate of 0.88 mm/yr. Converted to dry-weight values, the ~15–45% higher accumulation rate of Unit 3 is consistent with focused sedimentation (e.g. Blais and Kalff, 1995). Considering this tight link between core lithology and seismic stratigraphy, we extrapolated the core's age model to the deeper seismic sequence assuming a mean acoustic velocity of 1500 m/s for Units 1 to 6 (uppermost ~50 m) and 1550 m/s for Units 7 to 13 (~50–100 m sub-surface), in accordance with seismic velocities revealed for the lacustrine infill of crater lake Bosumtwi (Scholz et al., 2002; Schmitt et al., 2007). Based on the mean porosity gradient down-core (Fig. 6A), we then applied both a linear compaction correction of 0.18% per meter (cf. the value used for the upper 40 m of Lake Bosumtwi sediments; Brooks et al., 2005); and, alternatively, an exponential compaction correction according to the formula $\varphi = 88.849\ \exp(-2E{-}03\ z)$, with φ = porosity (%) and z = sub-surface depth (m). We retained the exponential compaction gradient for our reconstruction because it more closely simulates the natural behavior of sediments during burial. We note, however, that even at 100 m sub-bottom depth, the porosity values derived from both

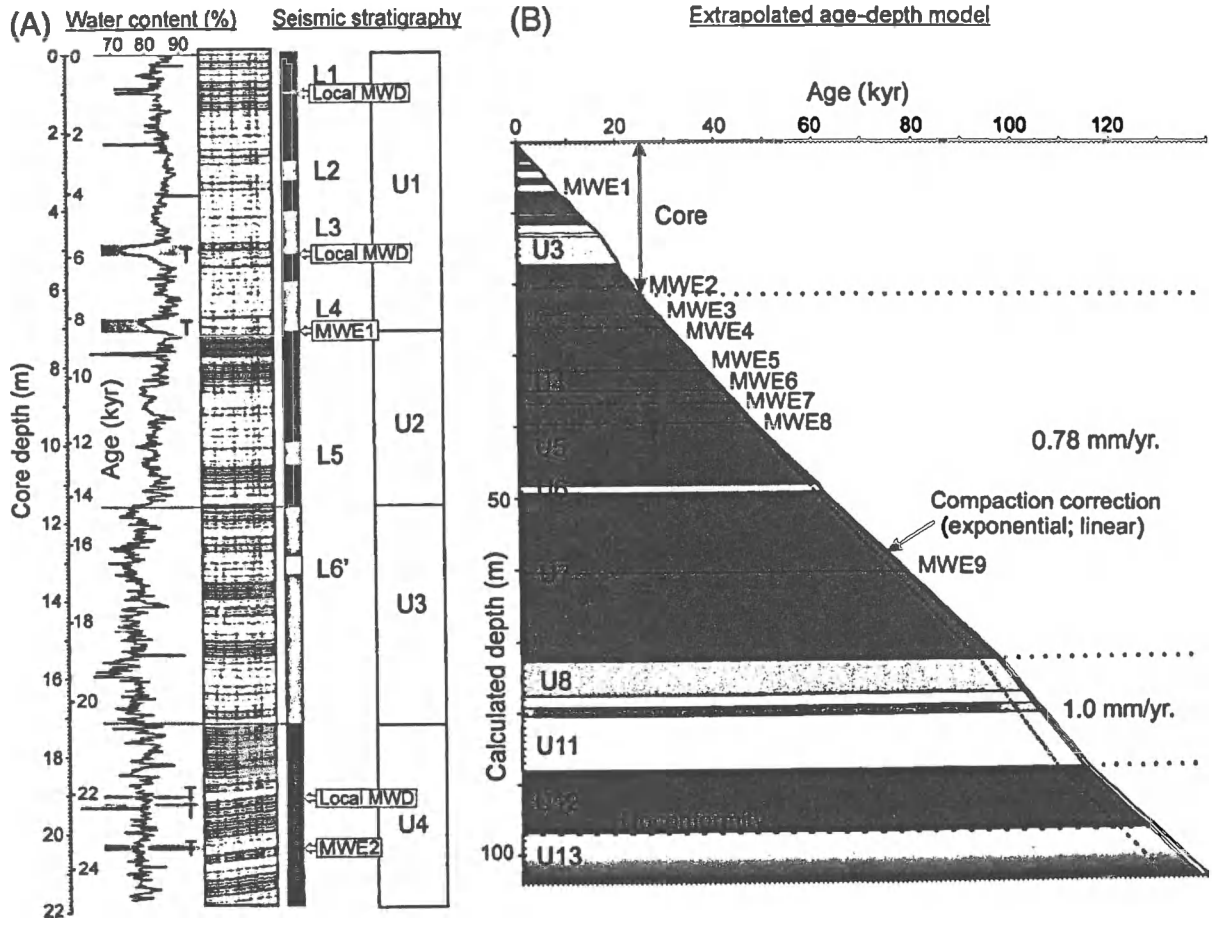

Fig. 6. A) Cross-correlation of the seismic sequence with core stratigraphy and age model, using as anchor points the water-content changes at the top and base of Unit 3, and the stratigraphic position of turbidite sections linked to MWDs and MWEs. B) Extrapolation of the core-based age model (25 kyr BP to present) to the seismic sequence to beyond the U12–U13 unconformity, without correction (dashed line) or with correction for estimated sediment compaction (black line: exponential; grey line: linear), and with sedimentation rates of individual seismic units deduced from their different mean sedimentation rates in the cored section. Grey-scale coding as in Figs. 3 and 6a.

models differ only ~1.9%; consequently their influence on the inferred chronology of seismic signatures is limited. Finally we adjusted the mean sedimentation rates of seismic units with different depositional geometry to the difference in sedimentation rate of ponded (U3) and draped units (U2 and U4; mean accumulation rate: 0.78 mm/yr) in the cored section. Fig. 6B shows the resulting age model for the Challa seismic sequence down to Unit 13 at ~100 m sub-bottom depth.

4. Lake-level reconstruction

Following other seismic-stratigraphic studies in fluctuating lakes (e.g. Bouroullec et al., 1991) we interpret the units of draped sedimentation (e.g., U1, U2, U4) to have been deposited during highstands and the units of basin-focused (ponded) sedimentation (e.g., U3) during lowstands. Among several sediment focusing processes that become effective at low lake level (Hilton, 1985), superficial sediments deposited in shallow areas during earlier highstands can be mobilized and re-deposited, resulting in a higher sedimentation rate in the basin centre. Similarly, the thin ponded lenses L1–L6′ within units U1–U3 are the expression of short-lived lowstands below the mean lake level represented by that unit.

The occurrence of basin-wide slope failures and fluid-escape features is also clearly related to lake-level fluctuation. When lake level drops, a temporary disequilibrium between confining pressure and pore pressure in low-permeability sediments can generate overpressure along discrete stratigraphic levels. These can then behave like a geotechnical 'weak layer', increasing the susceptibility of the slope sequence to gravitational failure. Such overpressures can also lead to focused fluid escape (Vendeville and Gaullier, 2003). Due to the bowl-shaped geometry of the Challa basin and the occurrence of numerous (undercompacted?) MWDs (cf. Chapron et al., 2004; Moernaut et al., 2009) these fluid escapes would have taken place at the basin periphery, possibly favoring local sublacustrine slope failure. Discharge of biogenic gas (probably methane) from uncompacted sediments during lake-level drops could have helped create the vertical conduits and pockmarks. Here, reduced confining pressure caused oversaturation of interstitial water and gas ebullition, strongly affecting slope stability (Vanoudheusden et al., 2004). Both of the above mechanisms are supported by the tight stratigraphic association (reflector r1) between MWE1 and widespread fluid escape at the highstand-to-lowstand transition U2/L4 (Fig. 5).

Earthquake shaking on its own is not likely to have triggered the recorded basin-wide slope failures in Lake Challa. In steep-sloped (10°–20°) glacigenic Alpine lakes with distinct lithological boundaries in the sedimentary slope sequence, earthquake shaking must reach Intensity VII (EMS98) to trigger basin-wide sublacustrine slope failure (Monecke et al., 2004). The basin-floor periphery of Lake Challa dips only 1°–5°, and the Mt. Kilimanjaro region lacks strong historical seismic activity (Hollnack and Stangl, 1998). However, less seismic acceleration may have sufficed to trigger slope failures during the periods of reduced slope stability caused by abrupt lake-level decline (e.g., Lee et al., 1996; Mullins and Halfman, 2001; Fanetti et al., 2008). Thus, for earthquake-triggered slope failure to occur in Lake Challa, overpressures induced by lake-level decline would seem to have been required. Anselmetti et al. (2009) proposed a similar link between lake-level fluctuation, earthquakes and sublacustrine slope failure for

mass-wasting during a major lowstand of Lake Potrok Aike (Argentina), a crater lake with similar dimensions as Lake Challa.

The proposed links between seismic-stratigraphic features, sedimentation dynamics and lake level are supported for the cored part of the Challa sequence by the timing of ponded Unit 3 (~20.5–14.5 kyr BP) during the LGM and early late-glacial period, and L5 (~12.9–12.0 kyr BP) during the Younger Dryas chronozone, two periods when most East African lakes are known to have experienced

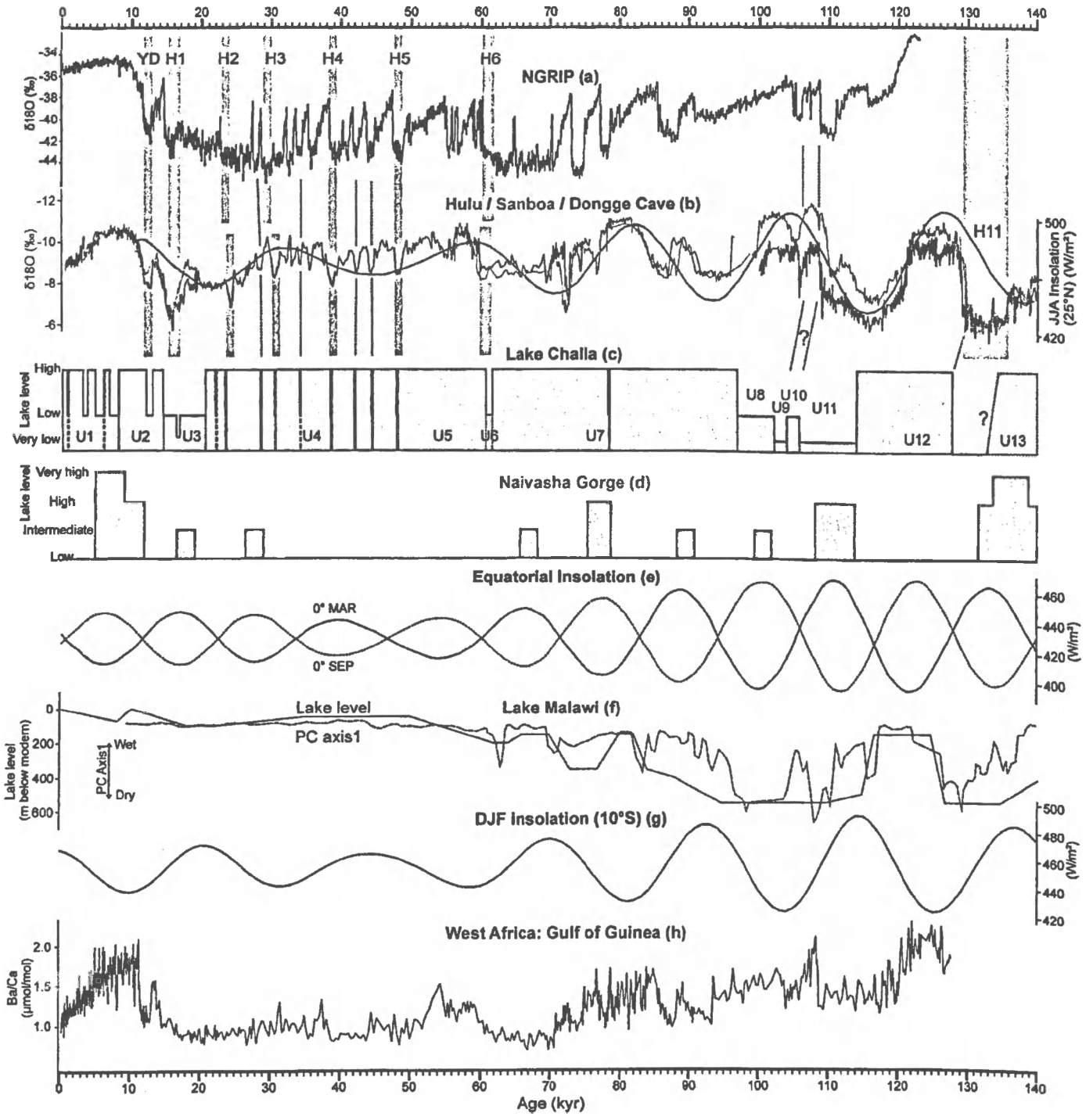

Fig. 7. Correlations (grey bars, dotted lines) between the 140-kyr lake-level reconstruction for Lake Challa and other records of orbital- and millennial-scale climate variability. a) The NGRIP ice-core record (Andersen and North Greenland Ice Core Project members, 2004); the timing of millennial-scale events in the last 42 kyr of this record has been updated (Svensson et al., 2006); see text. b) SE Asian speleothem records from the Hulu (Wang et al., 2001), Sanboa (Wang et al., 2008) and Dongge (Kelly et al., 2006) caves with mean summer insolation (June–July–August) at 25°N (Berger and Loutre, 1991). The originally higher Hulu and Dongge $\delta^{18}O$ values are plotted respectively 1.7‰ and 1.1‰ more negative compared to Sanboa data. c) Lake Challa lake-level record (this study). Blue line: ponded units and lenses. Red: MWE (full line) and local MWD (dashed line). d) Lake-level record from Naivasha Gorge, central Kenya Rift Valley (Bergner and Trauth, 2004). e) Mean March and September insolations on the equator (Berger and Loutre, 1991; Verschuren et al., 2009). f) Lake Malawi lake-level record according to seismic stratigraphy (full line; Scholz et al., 2007) and multivariate analysis of paleoecological proxies (dashed line; Cohen et al., 2007). g) Mean summer insolation at 10°S (December–January–February; Berger and Loutre, 1991). h) Ba/Ca record in Gulf of Guinea sediments (Weldeab et al., 2007) representing the history of the equatorial West African monsoon; higher Ba/Ca values reflect wetter conditions. Note that Lake Challa is situated to the south of Naivasha Gorge (Fig. 1), but is plotted above it for clarity of the correlation with NGRIP and the Asian speleothem records.

lowstands (Gasse et al., 2008). The thin ponded lens L6′ represents a short-lived 'extreme' lowstand below the mean level of U3 dated to ~16.9–16.3 kyr BP, i.e. within the H1 chronozone when also other East African lakes experienced extreme lowstands or fell dry (Stager et al., 2002; Lamb et al., 2007) and both the South and East Asian monsoon were substantially weakened (Wang et al., 2001; Shakun et al., 2007). The ponded lenses L4–L1 within U1 represent mid-Holocene lowstands, the timing of which is consistent with mid-Holocene drought recorded on Mt. Kenya (Barker et al., 2001). Further, the timing of Challa lake-level fluctuations reconstructed from seismic stratigraphy is in full agreement with variations in local monsoon rainfall inferred from the distribution of the organic biomarker index BIT in the Challa sediment core (Verschuren et al., 2009).

This climatic-hydrological validation of our seismic-stratigraphic inferences throughout the cored part (i.e. the last 25 kyrs) of the Challa sequence allows us to construct a lake-level curve for Lake Challa over the past 140 kyrs (Fig. 7). The accuracy of our chronology of past lake-level changes in Lake Challa during this period naturally depends on the validity of our assumptions about acoustic velocity, our compaction correction model, and whether sedimentation rates in the cored section are representative for the entire studied record. However, variation in these assumptions within reasonable limits does not substantially affect the inferred timing of events (Fig. 6B). After a long highstand period (U13), the lake desiccated completely shortly before ~128 kyr BP. We speculate that this drystand lasted only a few thousand years, because it caused only minor erosion and thin local packages of basin-focused sedimentation (Fig. 3: 'deepest part of paleobasin'). Around 128 kyr BP the basin filled rapidly, and lake level remained high (U12) until ~114 kyr BP when a major lake-level drop occurred. Very low levels (U11 and U9) persisted for at least 12 000 years, interrupted by a short-lived highstand dated to ~106–104 kyr BP (U10). From ~104 kyr BP onwards the lake rose gradually, attaining highstand conditions by ~97 kyr BP. This highstand persisted (U7, U5, and U4) until ~20.5 kyr BP (U3, the LGM lowstand), but was punctuated by short-lived lowstands at ~78 (MWE9), 61.5–60.5 (U6), 48 (MWE8), 44.5 (MWE7), 42 (MWE 6), 39 (MWE5), 34 (local MWD), 30.5 (MWE4), 28.5 (MWE3), 23.4 (MWE2) and 22.0 kyr BP (local MWD). We note that the exact relative magnitude of the associated lake-level changes in Lake Challa is uncertain, because draped sedimentation can occur over a wide range of lake depths.

5. A 140-kyr moisture-balance history

At first approximation, the lake-level history of Lake Challa reconstructed from seismic stratigraphy is influenced by local rainfall and run-off from the steep inner crater slopes, by temperature effects on evaporation from the lake surface and on evapotranspiration from the surrounding land surface, by the amount of sub-surface inflow, and by the sill elevation of significant outflow through porous crater walls. Temperature effects on evaporation or evapotranspiration are relatively limited in the case of Lake Challa, due to its very small local catchment area (Fig. 2A), its extremely low surface area-to-volume ratio (0.0128), and its near-constant surface area over the range of inferred lake-level fluctuation. Sub-surface inflow has probably always represented a major portion of the water budget, as it does today, but it responds quickly to changes in rainfall, because rain percolating through saturated forest soils on the upper slope of Mt. Kilimanjaro arrives at the lake within ~3 months (C. Wolff, GeoForschungsZentrum Potsdam, unpubl. data). Together with the established support from regional paleodata of the last 25 000 years, we therefore consider the Challa lake-level record an accurate reflection of the climatic moisture-balance history of equatorial East Africa.

Clear agreement between the inferred age of short-lived lake-level drops in Lake Challa between 60 and 20 kyr BP (Fig. 7) and that of Heinrich events recorded in Greenland (Svensson et al., 2006) and the Asian Monsoon domain (Wang et al., 2001) indicates that H6 is recorded as the 1-m thick ponded unit U6, and H5–H2 as respectively MWE8, MWE5, MWE4 and MWE2. Challa lake-level drops that are not readily attributable to H-events (e.g., MWE7 at ~44.5 kyr BP and MWE6 at ~42 kyr; Fig. 7) generally correspond to other discrete periods of weakened Asian Monsoon (Wang et al., 2001) during Greenland stadials (Andersen and North Greenland Ice Core Project members, 2004; Svensson et al., 2006). In this respect the Challa record supports the general link between millennial-scale behavior of the Indian Ocean monsoon and rapid D/O-related temperature fluctuations at high northern latitudes (Schulz et al., 1998), with severe H-event drought as the clearest climatic impact in equatorial East Africa (Tierney et al., 2008).

The two major lowstands at >128 and ~114–97 kyr BP imply regional drought considerably more severe than that which occurred during the LGM. Low-latitude precessional insolation forcing is an important regulator of hydrological change in the tropics at orbital time scales (Clement et al., 2004), but explaining the timing and duration of these two East African droughts by local (i.e., equatorial) insolation forcing (cf. Trauth et al., 2003) is not evident. The start (~114 kyr BP) and possibly the end (~97 kyr BP) of the U11–U8 lowstand in Lake Challa coincide with the 'megadrought' lowstand of Lake Malawi at 10°S (as recorded by sedimentological and paleoecological indicators; Fig. 7). There this MIS5 megadrought was explained to result from precession-forced monsoon failure (Scholz et al., 2007), matching modeling experiments (Clement et al., 2004) which suggest that when eccentricity is large, the amplitude of hydrological variability in the tropics caused by low-latitude precessional forcing is larger than that caused by glacial (i.e., high-latitude) forcing. However at Lake Challa near the equator we do not expect an equally strong precessional signature on rainfall, because anti-phased precessional insolation variation in the northern and southern hemispheres (Berger and Loutre, 1991; Fig. 7) predicts that negative insolation forcing of the northeasterly monsoon (bringing the 'short rains' to Lake Challa) would at any time be partly compensated by a positive forcing of the southeasterly monsoon (bringing the 'long rains' to Lake Challa; Verschuren et al., 2009). The strong 'megadrought' signature in the Challa record ~114–97 kyr BP thus indicates not only that the impact of an orbitally weakened northeasterly monsoon extended into equatorial East Africa, but also that the normally enhanced southeasterly monsoon was (partly) failing during this period (Fig. 7). Still, possible temporal correspondence of the lesser lowstand (inferred modestly wet period) dated to ~106–104 kyr BP in Lake Challa (U10; or ~107–105 kyr BP using the linear compaction correction; see Fig. 6) and to ~108–105 kyr BP in Lake Malawi (Cohen et al., 2007) with peak East Asian monsoon intensity (Kelly et al., 2006) and Greenland warming (Andersen and North Greenland Ice Core Project members, 2004) at 109–106 kyr BP suggests that high-latitude influence on monsoon dynamics in the western Indian Ocean continued without interruption.

The age and rather short duration of the Lake Challa desiccation ending at ~128 kyr BP (or ~130 kyr BP; Fig. 6) suggest that this episode of extreme drought at the equator may represent a strong regional impact of H11, which is known to have substantially weakened the East Asian monsoon (Kelly et al., 2006). In Lake Malawi (10°S) the combined drying effect of a rain-season insolation minimum, peak penultimate glaciation and H11 at that time appears to have been comparable to the ~110–95 kyr BP megadrought (Scholz et al., 2007; Cohen et al., 2007), but at Lake Challa's latitude (3° S), H11 helped create the most extreme drought of the past 140 kyr.

The overall reduction in precession-driven moisture variability through the last glacial cycle, as observed in the Malawi and Challa records, is explained by the moderating effect of low orbital

eccentricity on the amplitude of precessional insolation forcing, supplemented by changes in the tropical hydrological cycle under glacial-period boundary conditions (Clement et al., 2004). In the Lake Challa region it created near-continuous moist climate conditions from ~97 kyr BP (or ~98 kyr BP; Fig. 6) to 20.5 kyr BP, i.e. throughout the latter part of MIS5, MIS4 and MIS3. The generally humid climate and ecosystems which prevailed in easternmost equatorial Africa during the later part of the last glacial cycle (this study), as well as in southeastern tropical Africa (Scholz et al., 2007; Cohen et al., 2007; Mumbi et al., 2008) can also have resulted in part because modest glacial cooling of the southern tropical Indian Ocean (1.5–2.0 °C relative to today; Pinot et al., 1999) maintained adequate moisture flux onto adjacent portions of the African continent (Goddard and Graham, 1999; Marchant et al., 2006). This wet glacial climate on the Indian Ocean side of tropical Africa contrasts with the main trend toward increasing glacial aridity since ~70 kyr BP (early MIS4) documented from its Atlantic side (Dupont et al., 2000; Weldeab et al., 2007); sustained glacial aridity during MIS3 appears to even swamp the local impact of super-imposed H-event droughts (Weldeab et al., 2007). In parts of central and eastern tropical Africa receiving both Atlantic and Indian Ocean moisture, more or less sustained glacial drought sets in at the intermediate time of ~36–32 kyr BP (Bonnefille and Chalie, 2000; Felton et al., 2007; Tierney et al., 2008), i.e. during the later part of MIS3. To the north of Lake Challa a progressive drying trend from MIS4 to MIS3 may even have been manifested as far east as the eastern Rift Valley in Kenya (36°E), if the discontinuous nature of the long-term hydrological record available from Lake Naivasha (Bergner and Trauth, 2004; Fig. 7) allows this inference. Since also today moisture sourced in the Atlantic and Indian Oceans converges over the East African Plateau during much of the year (Fig. 1), naturally the climate history of much of tropical Africa bears a strong Atlantic signature. Accumulating evidence for a major west-to-east gradient in glacial-period moisture balance across tropical Africa underscores the relative independence of western Indian Ocean monsoon dynamics from high-latitude boundary conditions. This contrasts with the Atlantic Ocean domain, where important latitudinal heat redistribution by the meridional overturning circulation more tightly couples tropical climate history to the history of northern high-latitude glaciation. The long period of moist glacial climate and short, somewhat modest LGM drought which appears to have characterized easternmost equatorial and southeastern tropical Africa created conditions of relative environmental stability during much of the last 100 000 years. This may have helped maintain through time (Mumbi et al., 2008) the unusually high biological diversity now characterizing the region's tropical forest ecosystems, in particular those of the Eastern Arc mountains in Tanzania (Myers et al., 2000).

Acknowledgements

This work was sponsored by FWO-Vlaanderen projects 3G0086.00 and 3G0641.05 (the latter administered through the ESF-EUROCORES programme EuroCLIMATE). Fieldwork was conducted with research permission of the Kenyan Ministry of Education and Science to DV (MOEST 13/001/11C). We thank W. Versteeg and K. De Rycker for the acquisition of the seismic data, and the CHALLACEA team for the stimulating discussions. JM acknowledges the support of the Institute for the Promotion of Innovation through Science and Technology in Flanders (IWT-Vlaanderen).

Appendix A. Supplementary data

Supplementary data associated with this article can be found, in the online version, at doi:10.1016/j.epsl.2009.12.023.

References

Andersen, K.K., North Greenland Ice Core Project members, 2004. High-resolution record of Northern Hemisphere climate extending into the last interglacial period. Nature 431, 147–151.

Anselmetti, F.S., Ariztegui, D., De Batist, M., Gebhardt, A.C., Haberzettl, T., Niessen, F., Ohlendorf, C., Zolitschka, B., 2009. Environmental history of southern Patagonia unravelled by the seismic stratigraphy of Laguna Potrok Aike. Sedimentology 56 (4), 873–892.

Barker, P.A., Street-Perrott, F.A., Leng, M.J., Greenwood, P.B., Swain, D.L., Perrott, R.A., Telford, R.J., Ficken, K.J., 2001. A 14,000-year oxygen isotope record from diatom silica in two alpine lakes on Mt. Kenya. Science 292, 2307–2310.

Berger, A., Loutre, M.F., 1991. Insolation values for the climate of the last 10 million years. Quat. Sci. Rev. 10, 297–317.

Bergner, A.G.N., Trauth, M.H., 2004. Comparison of the hydrological and hydrochemical evolution of Lake Naivasha (Kenya) during three highstands between 175 and 60 kyr BP. Palaeogeogr. Palaeoclimatol. Palaeoecol. 215, 17–36.

Blais, J.M., Kalff, J., 1995. The influence of lake morphometry on sediment focusing. Limnol. Oceanogr. 40 (3), 582–588.

Bonnefille, R., Chalie, F., 2000. Pollen-inferred precipitation time-series from equatorial mountains, Africa, the last 40 kyr BP. Glob. Planet. Change 26 (1–3), 25–50.

Bouroullec, J.-L., Rehault, J.-P., Rolet, J., Tiercelin, J.-J., Mondeguer, A., 1991. Quaternary sedimentary processes and dynamics in the northern part of the lake Tanganyika Trough, East African rift system. Evidence of lacustrine eustatism? Bull. des Centre de Recherches Exploration–Production Elf-Aquitaine 15 (2), 343–368.

Brooks, K., Scholz, C.A., King, J.W., Peck, J., Overpeck, J.T., Russell, J.M., Amoako, P.Y.O., 2005. Late-Quaternary lowstands of lake Bosumtwi, Ghana: evidence from high-resolution seismic-reflection and sediment-core data. Palaeogeogr. Palaeoclimatol. Palaeoecol. 216, 235–249.

Brown, E.T., Johnson, T.C., Scholz, C.A., Cohen, A.S., King, J.W., 2007. Abrupt change in tropical African climate linked to the Bipolar Seesaw over the past 55,000 years. Geophys. Res. Lett. 34, L20702 doi:10.1029/2007GL031240.

Chapron, E., Van Rensbergen, P., De Batist, M., Beck, C., Henriet, J.P., 2004. Fluid-escape features as a precursor of a large sublacustrine sediment slide in Lake Le Bourget, NW Alps, France. Terra Nova 16, 305–311.

Clement, A.C., Hall, A., Broccoli, A.J., 2004. The importance of precessional signals in the tropical climate. Clim. Dynamics 22, 327–341.

Cohen, A.S., Stone, J.R., Beuning, K.R.M., Park, L.E., Reinthal, P.N.R., Dettman, D., Scholz, C.A., Johnson, T., King, J.W., Talbot, M.R., Brown, E.T., Ivory, S.J., 2007. Ecological consequences of Early Late-Pleistocene megadroughts in tropical Africa. PNAS 104, 16422–16427.

Dupont, L.M., Jahns, S., Marret, F., Ning, S., 2000. Vegetation change in equatorial West Africa: time slices for the last 150 ka. Palaeogeogr. Palaeoclimatol. Palaeoecol. 155, 95–122.

Fanetti, D., Anselmetti, F.S., Chapron, E., Sturm, M., Vezzoli, L., 2008. Megaturbidite deposits in the Holocene basin fill of Lake Como (Southern Alps, Italy). Palaeogeogr. Palaeoclimatol. Palaeoecol. 259 (2–3), 323–340.

Felton, A.A., Russell, J.M., Cohen, A.S., Baker, M.E., Chesley, J.T., Lezzar, K.E., McGlue, M.M., Pigati, J.S., Quade, J., Stager, J.C., Tiercelin, J.J., 2007. Paleolimnological evidence for the onset and termination of glacial aridity from Lake Tanganyika, tropical East Africa. Palaeogeogr. Palaeoclimatol. Palaeoecol. 252, 405–423.

Ganopolski, A., Rahmstorf, S., 2001. Rapid changes of glacial climate simulated in a coupled climate model. Nature 409, 153–158.

Gasse, F., Chalié, F., Vincens, A., Williams, M.A.J., Williamson, D., 2008. Climatic patterns in equatorial and southern Africa from 30,000 to 10,000 years ago reconstructed from terrestrial and near-shore proxy data. Quat. Sci. Rev. 27, 2316–2340.

Goddard, L., Graham, N.E., 1999. Importance of the Indian Ocean for simulating rainfall anomalies over eastern and southern Africa. J. Geophys. Res. 104, 19099–19116.

Hilton, J., 1985. A conceptual framework for predicting the occurrence of sediment focusing and sediment redistribution in small lakes. Limnol. Oceanogr. 30 (6), 1131–1143.

Hollnack, D., Stangl, R., 1998. The seismicity related to the southern part of the Kenya Rift. J. Afr. Earth Sci. 26 (3), 477–495.

Kelly, M.J., Edwards, R.L., Cheng, H., Yuan, D., Cai, Y., Zhang, M., Lin, Y., An, Z., 2006. High resolution characterization of the Asian Monsoon between 146,000 and 99,000 years B.P. from Dongge Cave, China and global correlation of events surrounding Termination II. Palaeogeogr. Palaeoclimatol. Palaeoecol. 236, 20–38.

Lamb, H.F., Bates, C.R., Coombes, P.V., Marshall, M.H., Umer, M., Davies, S.J., Dejen, E., 2007. Late Pleistocene desiccation of Lake Tana, source of the Blue Nile. Quat. Sci. Rev. 26 (3–4), 287–299.

Lee, H.J., Chough, S.K., Yoon, S.H., 1996. Slope-stability change from late Pleistocene to Holocene in the Ulleung Basin, East Sea (Japan Sea). Sediment. Geol. 104 (1–4), 39–51.

Marchant, R., Mumbi, C., Behera, S., Yamagata, T., 2006. The Indian Ocean Dipole – the unsung driver of climatic variability in East Africa. Afr. J. Ecol. 45, 4–16.

McGlue, M.M., Lezzar, K.E., Cohen, A.S., Russell, J.M., Tiercelin, J.-J., Felton, A.A., Mbede, E., Nkotagu, H.H., 2008. Seismic records of late Pleistocene aridity in Lake Tanganyika, tropical East Africa. J. Paleolimnol. 40 (2), 635–653.

McManus, J.F., Francois, R., Gherardi, J.-M., Keigwin, L.D., Brown-Leger, S., 2004. Collapse and rapid resumption of Atlantic meridional circulation linked to deglacial climate changes. Nature 428, 834–837.

Moernaut, J., De Batist, M., Heirman, K., Van Daele, M., Pino, M., Brummer, R., Urrutia, R., 2009. Fluidization of buried mass-wasting deposits in lake sediments and its relevance for paleoseismology: results from a reflection seismic study of lakes Villarrica and Calafquén (South-Central Chile). Sediment. Geol. 213 (3–4), 121–135.

Moernaut, J., De Batist, M., submitted for publication. Morphometric and seismic-stratigraphic analysis of 96 sublacustrine landslides: implications for the processes leading to frontally emergent and frontally confined subaqueous landslides. Mar. Geol.

Monecke, K., Flavio, S., Anselmetti, F., Becker, A., Sturm, M., Giardini, D., 2004. The record of historic earthquakes in lake sediments of Central Switzerland. Tectonophysics 394, 21–40.

Mullins, H.T., Halfman, J.D., 2001. High-resolution seismic reflection evidence for middle Holocene environmental change, Owasco Lake, New York. Quat. Res. 55 (3), 322–331.

Mumbi, C.T., Marchant, R., Hooghiemstra, H., Wooller, M.J., 2008. Late Quaternary vegetation reconstruction from the Eastern Arc Mountains, Tanzania. Quat. Res. 69, 326–341.

Myers, N., Mittermeier, R.A., Mittermeier, C.G., da Fonseca, G.A.B., Kent, J., 2000. Biodiversity hotspots for conservation priorities. Nature 403, 853–858.

Payne, B.R., 1970. Water balance of lake Challa and its relation to groundwater from Tritium and stable isotope data. J. Hydrol. 11, 47–58.

Pinot, S., Ramstein, G., Harrison, S.P., Prentice, I.C., Guiot, J., Stute, M., Joussaume, S., 1999. Tropical paleoclimates at the Last Glacial Maximum: comparison of Paleoclimate Modeling Intercomparison Project (PMIP) simulations and paleodata. Clim. Dynamics 15 (11), 857–874.

Scholz, C.A., Johnson, T.C., Cohen, A.S., King, J.W., Peck, J.A., Overpeck, J.T., Talbot, M.R., Brown, E.T., Kalindekafe, L., Amoako, P.Y.O., Lyons, R.P., Shanahan, T.M., Castaneda, I.S., Heil, C.W., Forman, S.L., McHargue, L.R., Beuning, K.R., Gomez, J., Pierson, J., 2007. East African megadroughts between 135 and 75 thousand years ago and bearing on early-modern human origins. PNAS doi:10.1073/pnas.0703874104.

Scholz, C.A., Karp, T., Brooks, K.M., Milkereit, B., Amoako, P.Y.O., Arko, J.A., 2002. Pronounced central uplift identified in the Bosumtwi impact structure, using multichannel seismic reflection data. Geology 30 (10), 939–942.

Scholz, C.A., King, J.W., Ellis, G.S., Swart, P.K., Stager, J.C., Colman, S.M., 2003. Paleolimnology of Lake Tanganyika, East Africa, over the past 100 kyr. J. Paleolimnol. 30, 139–150.

Schulz, H., von Rad, U., Erlenkeuser, H., 1998. Correlation between Arabian Sea and Greenland climate oscillations of the past 110,000 years. Nature 393, 54–57.

Schmitt, D.R., Milkereit, B., Karp, T., Scholz, C.A., Danuor, S., Meillieux, D., Welz, M., 2007. In situ seismic measurements in borehole LB-08A in the Bosumtwi impact structure, Ghana: preliminary interpretation. Meteor. Planet. Sci. 42 (4/5), 755–768.

Shakun, J.D., Burns, S.J., Fleitmann, D., Kramers, J., Matter, A., Al-Subary, A., 2007. A high-resolution, absolute-dated deglacial speleothem record of Indian Ocean climate from Socotra Island, Yemen. Earth Planet. Sci. Lett. 259 (3–4), 442–456.

Stager, J.C., Mayewski, P.A., Meeker, L.D., 2002. Cooling cycles, Heinrich event 1, and the desiccation of Lake Victoria. Palaeogeogr. Palaeoclimatol. Palaeoecol. 183 (1–2), 169–178.

Svensson, A., Andersen, K.K., Bigler, M., Clausen, H.B., Dahl-Jensen, D., Davies, S.W., Johnsen, S.J., Muscheler, R., Rasmussen, S.O., Rothlisberger, R., Steffensen, J.P., Vinther, B.M., 2006. The Greenland Ice core chronology 2005, 15–42 ka. Part 2: comparison to other records. Quat. Sci. Rev. 25, 3258–3267.

Thomas, D.S.G., Bailey, R., Shaw, P.A., Durcan, J.A., Singarayer, J.S., 2009. Late Quaternary highstands at Lake Chilwa, Malawi: frequency, timing and possible forcing mechanisms in the last 44 ka. Quat. Sci. Rev. 28 (5–6), 526–539.

Tierney, J.E., Russell, J.M., Huang, Y., Sinninghe Damsté, J.S., Hopmans, E.C., Cohen, A.S., 2008. Northern Hemisphere controls on tropical southeast African climate during the past 60,000 years. Science 322, 252–255.

Tjallingii, R., Claussen, M., Stuut, J.-B.W., Fohlmeister, J., Jahn, A., Bickert, T., Lamy, F., Röhl, U., 2008. Coherent high- and low-latitude control of the northwest African hydrological balance. Nat. Geosci. 1, 670–675.

Trauth, M.H., Deino, A.L., Bergner, A.G.N., Strecker, M.R., 2003. East African climate change and orbital forcing during the last 175 kyr BP. Earth Planet. Sci. Lett. 206, 297–313.

Vanoudheusden, E., Sultan, N., Cochonat, P., 2004. Mechanical behaviour of unsaturated marine sediments: experimental and theoretical approaches. Mar. Geol. 213, 323–342.

Vendeville, B.C., Gaullier, V., 2003. Role of pore-fluid pressure and slope angle in triggering submarine mass movements: natural examples and pilot experimental models. In: Locat, J., Mienert, J. (Eds.), Submarine Mass Movements and their Consequences, First International Symposium. Kluwer Academic Publishers, Netherlands, pp. 137–144.

Verschuren, D., Sinninghe Damsté, J., Moernaut, J., Kristen, I., Blaauw, M., Fagot, M., Haug, G., van Geel, B., De Batist, M., Barker, P., Vuille, M., Conley, D., Olago, D.O., Milne, I., Plessen, B., Eggermont, H., Wolff, C., Hurrell, E., Ossebaar, J., Lyaruu, A., van der Plicht, J., Cumming, B.F., Brauer, A., Rucina, S.M., Russell, J.M., Keppens, E., Hus, J., Bradley, R.S., Leng, M., Mingram, J., Nowaczyk, N.R., 2009. Half-precessional dynamics of monsoon rainfall near the East African equator. Nature 462, 637–641.

Wang, Y., Cheng, H., Edwards, R.L., An, Z.S., Wu, J.Y., Shen, C.-C., Dorale, J.A., 2001. A high-resolution absolute-dated Late Pleistocene monsoon record from Hulu Cave, China. Science 294, 2345–2348.

Wang, Y., Cheng, H., Edwards, R.L., Kong, X., Shao, X., Chen, S., Wu, J., Jiang, X., Wang, X., An, Z., 2008. Millennial- and orbital-scale changes in the East Asian monsoon over the past 224,000 years. Nature 451, 1090–1093.

Weldeab, S., Lea, D.W., Schneider, R.R., Andersen, N., 2007. 155,000 years of West African monsoon and ocean thermal evolution. Science 316, 1303–1307.

Yuan, D., Cheng, H., Edwards, R.L., Dykoski, C.A., Kelly, M.J., Zhang, M., Qing, J., Lin, Y., Wang, Y., Wu, J., Dorale, J.A., An, Z., Cai, Y., 2004. Timing, duration, and transitions of the last Interglacial Asian monsoon. Science 304, 575–578.